JACS
JOURNAL OF THE AMERICAN CHEMICAL SOCIETY

Article

pubs.acs.org/JACS

Influenza Virus A M2 Protein Generates Negative Gaussian Membrane Curvature Necessary for Budding and Scission

Nathan W. Schmidt,[†] Abhijit Mishra,[§,⊥] Jun Wang,[‡,⊥] William F. DeGrado,*[,‡] and Gerard C. L. Wong*[,†]

[†]Department of Bioengineering, University of California, Los Angeles, Los Angeles, California 90095, United States
[§]Metallurgy & Materials Science Department, IIT Gandhinagar, Ahmedabad, 382424, Gujarat, India
[‡]Department of Pharmaceutical Chemistry, University of California, San Francisco, San Francisco, California 94158, United States

Supporting Information

ABSTRACT: The M2 protein is a multifunctional protein, which plays several roles in the replication cycle of the influenza A virus. Here we focus on its ability to promote budding of the mature virus from the cell surface. Using high-resolution small-angle X-ray scattering we show that M2 can restructure lipid membranes into bicontinuous cubic phases which are rich in negative Gaussian curvature (NGC). The active generation of negative Gaussian membrane curvature by M2 is essential to influenza virus budding. M2 has been observed to colocalize with the region of high NGC at the neck of a bud. The structural requirements for scission are even more stringent than those for budding, as the neck must be considerably smaller than the virus during 'pinch off'. Consistent with this, the amount of NGC in the induced cubic phases suggests that M2 proteins can generate high curvatures comparable to those on a neck with size 10× smaller than a spherical influenza virus. Similar experiments on variant proteins containing different M2 domains show that the cytoplasmic amphipathic helix is necessary and sufficient for NGC generation. Mutations to the helix which reduce its amphiphilicity and are known to diminish budding attenuated NGC generation. An M2 construct comprising the membrane interactive domains, the transmembrane helix and the cytoplasmic helix, displayed enhanced ability to generate NGC, suggesting that other domains cooperatively promote membrane curvature. These studies establish the importance of M2-induced NGC during budding and suggest that antagonizing this curvature is a viable anti-influenza strategy.

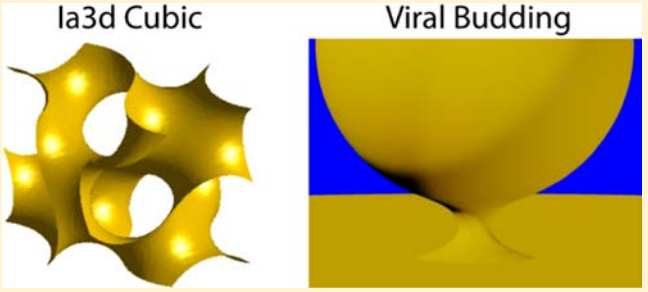

INTRODUCTION

Budding from cells is an essential step in the replication cycle of enveloped viruses. This complex process requires the organized deformation of the cellular membrane and necessarily involves localized regions of specific types of high membrane curvature. To facilitate budding many enveloped RNA viruses, such as HIV and the Ebola virus, commandeer cellular machinery like proteins from the host endosomal sorting complex required for transport (ESCRT) pathway that can induce membrane budding and scission and are normally employed in multivesicular body (MVB) biogenesis, cytokinesis, and autophagy.[1−3] An increasing body of evidence suggests that the influenza virus can facilitate its own egress through ESCRT-independent mechanisms[1,4] and, therefore, might be equipped with machinery that can generate the types of membrane curvatures required for viral budding and scission.

Recent studies have shown that the influenza A virus M2 protein plays a pivotal role in mediating viral budding and scission.[5] M2 is a 97 amino acid integral membrane protein which associates into a homotetramic proton selective ion channel and is known to play multiple roles during the infectious cycle of the virus (Figure 1).[6] The multifunctional abilities of M2 are conferred by distinctive domains which encode one or multiple functions. M2 contains a 24 residue (1−24) N-terminal extracellular domain that is important for incorporation into the virion of the influenza A virus.[7] Residues 25−46 comprise the α-helical transmembrane (TM) domain that is necessary and sufficient for tetramerization into a proton selective ion channel. This domain is essential for the virus uncoating process and subsequent virus−endosome membrane fusion and escape.[7] It is also the binding site of amantadine and rimantadine.[8−11] The TM domain is followed by a 15-residue long (47−61) C-terminal cytoplasmic (C-cyto) amphipathic membrane-associated helix that is involved in cholesterol binding,[12] membrane localization, budding, and scission.[5] Finally, there is an unstructured C-terminal tail (62−97) that interacts with matrix protein M1.[13]

Experimental evidence for the role of the M2 C-cyto domain in viral budding and scission comes from *in vitro* demonstrations that both the M2 protein as well as its C-cyto helix are capable of inducing budding in giant unilamellar vesicles, as well as *in vivo* assays which showed that M2 can cause budding out of cells.[5] The general reduction of budding and scission ability from replacements of key hydrophobic residues with alanine in the M2 C-cyto domain further validates

Received: January 6, 2013
Published: August 20, 2013

   dx.doi.org/10.1021/ja400146z | J. Am. Chem. Soc. 2013, 135, 13710−13719

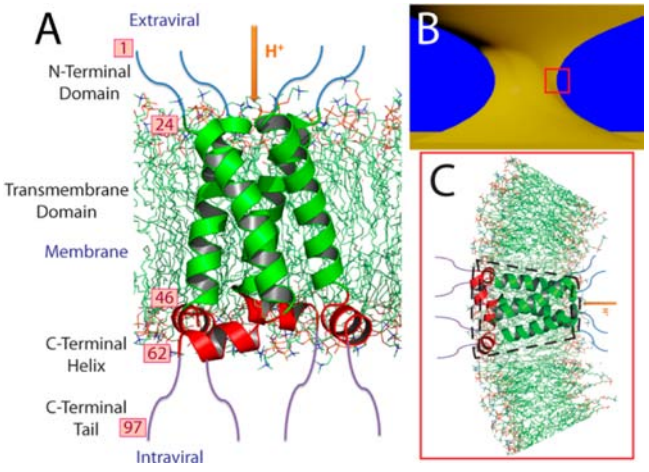

Figure 1. The influenza A virus M2 protein has an essential role in viral budding and scission. (A) Domain structure model of influenza A virus M2 proton channel. Model is based on ref 14. (B) Illustration of the neck in a bud. (C) Close up view illustrating an M2 channel on the neck region corresponding to the red box in (B). M2 generates membrane curvature via its C-terminal amphipathic helix as well as from the volume excluded by the membrane-associated regions of the channel (outlined by dashed lines).

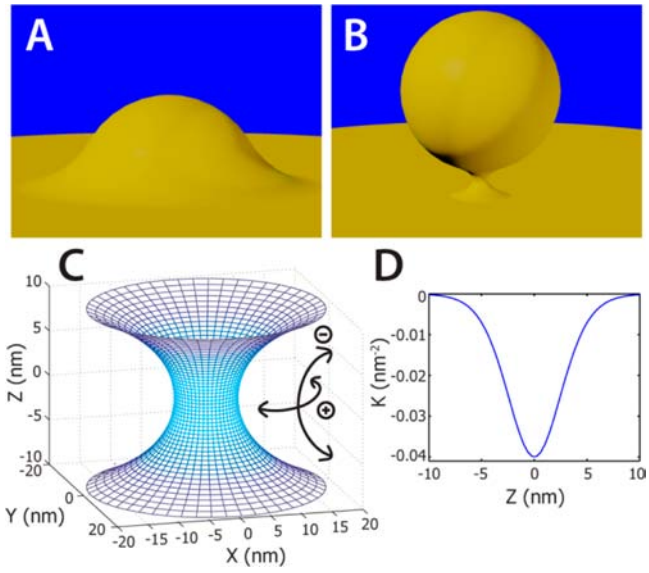

Figure 2. Influenza A viral budding and scission is mediated by the M2 protein. (A) Illustration of an early stage in the budding process when the emerging virion begins to protrude out of the cytoplasmic membrane. The M2 protein localizes to the base of the protrusion which has NGC (positive curvature around the bump and initial negative curvature up the bump). As the bud progresses, the virus emerges as the base constricts into a neck with higher NGC. (B) Late stage in the budding process just before membrane scission. The virus is approximated as a sphere with a diameter that is 10× the size of the width of the constricted neck. (C) A catenoid surface with 10 nm width at its narrowest cross-section, $Z = 0$ nm. The shape of the neck will conform to a catenoid, a minimal surface which has zero mean curvature and NGC everywhere. Arrows show directions of positive and negative curvature. (D) Negative Gaussian curvature, K, along the vertical direction of the neck in (C). The K-values on the surface of this catenoid are similar to those extracted from the bicontinuous cubic phases that M2 proteins generated in membranes.

the importance of the amphipathic helix in generating membrane curvature as well as shows that curvature generation is sensitive to certain physicochemical properties, such as hydrophobicity.[5] Moreover, the predominant localization of M2 to the neck of budding virions (Figure 1) suggests there is a relationship between its location on the membrane and its ability to generate the types of membrane curvature which assist in the completion of viral budding and scission (Figure 2A,B).[5,15] These studies clearly show that M2 plays a role in generating membrane curvature and that this ability is largely conferred by its C-cyto domain. A detailed characterization of the structure and interactions in M2−lipid complexes can provide explanations for how the composition of the C-cyto domain imparts M2 with the ability to generate specific types of membrane curvatures and how these curvatures facilitate virion release. In principle, this knowledge provides guidelines for the design of budding proteins as well as suggests new drug targets for influenza which can assist in the development of therapeutic strategies for the next generation of antiflu drug designs and combination chemotherapies.

In this work we use synchrotron small-angle X-ray scattering (SAXS) to characterize the membrane curvature deformations induced by WT Udorn full length M2, along with variants including the C-cyto domain, a peptide consisting of TM + C-cyto helices (M2TM-cyto), and their corresponding penta-Ala mutants (see Figure S1 for sequences). The M2 protein has been structurally characterized in a variety of membrane environments.[6,16−20] Here we focus on its ability to generate membrane curvature. By varying the biophysical properties of the membrane via changes in lipid composition, we quantitatively measure the curvature deformations induced by the native M2 protein and its variants and relate the types of membrane curvature they generate to their known abilities to promote budding and scission. In general, the native M2 protein and its variants are able to generate bicontinuous cubic phases rich in bilayer negative Gaussian curvature (NGC), the type of curvature necessary for a variety of membrane destabilizing processes including budding and scission. The structural requirements for scission are even more stringent than those for budding, as the radius of the neck must be considerably smaller than the radius of the virus during 'pinch off'. Consistent with this role, the range of observed NGC in the M2-induced cubic phases is similar to the distribution of this curvature on the neck of a bud one-tenth the size of a spherical influenza virus. This observation is interesting, since previous work[21] has shown that insertion of amphipathic helices with similar compositions to the M2 C-cyto helix by proteins like epsins can lead to membrane scission, while BAR domains that do not have such helices stabilize 'necks' that conform to the concave domain.

Importantly, generation of NGC tracked with activity profiles. Substitution of five bulky hydrophobic amino acids with alanines on the nonpolar face of the C-cyto amphipathic α-helix reduced the range of lipid compositions where cubic phases were observed, consistent with previous structure−activity studies which showed that reducing C-cyto helix hydrophobicity diminishes budding and scission ability.[5] While the C-cyto helix itself was sufficient to generate NGC, both the full length M2 protein and the M2TM-cyto peptide generated cubic phases over a wider range of lipid compositions. The enhancement of NGC from the presence of other domains in the M2 protein implies that although the C-cyto domain is primarily responsible for inducing curvature, other portions of the protein can enhance curvature generation via protein shape

dx.doi.org/10.1021/ja400146z | J. Am. Chem. Soc. 2013, 135, 13710−13719

effects. Because NGC is necessary for virion release, antagonizing this type of membrane curvature is a viable therapeutic strategy and drugs which can 'turn-off' NGC have potential as antiviral agents.

RESULTS AND DISCUSSION

SAXS Study Shows M2 Proteins Can Generate NGC in Lipid Membranes. To investigate the membrane deformations induced by M2, small unilamellar vesicles (SUVs) were incubated with the full length protein, and the resulting liquid crystalline structures were characterized by SAXS. In DOPE/DOPS = 80/20 membranes, three different sets of correlation peaks were observed (Figure 3A): (1) A set with characteristic

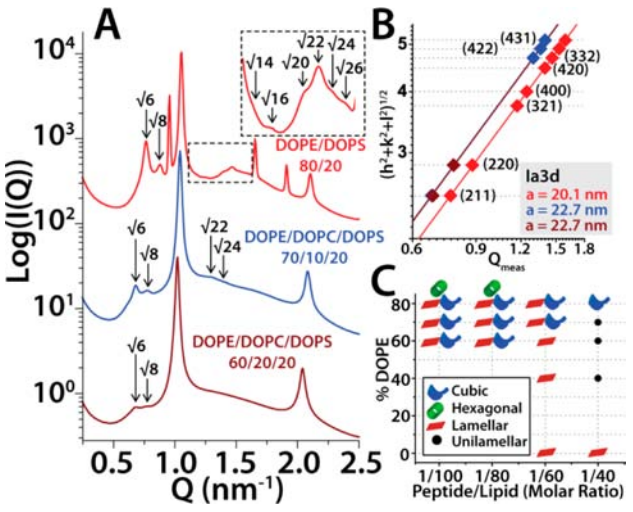

Figure 3. The M2 protein generated NGC in phospholipid membranes. (A) SAXS spectra from DOPE/DOPC/DOPS = X/(80 − X)/20 vesicles incubated with M2 at 1/100 protein to lipid (P/L) molar ratio. M2 induced Ia3d cubic phases in membranes with DOPE content as low as X = 60%. Overall, negative intrinsic curvature lipids promoted nonlamellar phase formation as indicated by the appearance of higher reflections from the Ia3d at elevated DOPE and the presence of an inverted hexagonal phase in 80% DOPE membranes. The inset provides a more detailed view of the higher order Ia3d phase reflections. (B) Log−log plots of the assigned reflections versus the measured Q-positions for Ia3d cubic peaks in the three spectra from (A). For powder averaged cubic phases $Q_{(hkl)} = 2\pi\sqrt{(h^2 + k^2 + l^2)}/a$, where h, k, and l are the Miller indices and a is the lattice parameter. The calculated lattice parameters, extracted using linear trendline fits, are the same color as the spectra in (A). Left-shifted trendlines indicate larger cubic phase lattice parameters. (C) Phase diagram for M2 protein with ternary DOPE/DOPC/DOPS membranes. The symbols show which phases were observed for a given %DOPE and P/L ratio. In PE-rich membranes nonlamellar cubic and inverted hexagonal phases were prominent, whereas lamellar phases were dominant in reduced DOPE membranes.

Q-ratios $\sqrt{6}$:$\sqrt{8}$:$\sqrt{14}$:$\sqrt{16}$:$\sqrt{20}$:$\sqrt{22}$:$\sqrt{24}$, which indexes (Figure 3B) to a Ia3d cubic 'gyroid' phase[22,23] with lattice parameter a_{Ia3d} = 20.1 nm (see Materials and Methods for indexing procedures and Tables S2−S8 in SI for lattice parameters for all observed phases in this study, and their average NGCs, <K>). (2) One with Q-ratios $\sqrt{1}$:$\sqrt{3}$:$\sqrt{4}$:$\sqrt{7}$, which indicates the presence of an inverted hexagonal (H_{II}) phase with lattice parameter a_{Hex} = 7.60 nm. (3) One with integral Q-values 1:2, consistent with a lamellar (L_α) phase with lattice parameter d = 5.98 nm. The Ia3d is a bicontinuous cubic phase where the lipid bilayer separates space into two equivalent but nonintersecting regions of water channels with three branches at each junction.[23] The center of the bilayer traces out a minimal surface with principle axes of curvature, c_1 and c_2, that are equal and opposite at every point ($c_1 = -c_2$). Such surfaces have zero mean curvature, $H = 1/2(c_1 + c_2) = 0$, and NGC, $K = c_1{*}c_2 < 0$ everywhere, and locally have a saddle shape. Negative Gaussian curvature (also known as saddle-splay curvature) is present at the 'neck' of protrusions (Figure 2A,B),[24] the region where M2 is known to localize during the budding process,[5] and increasing amounts of NGC are required to pinch off the nascent virion from the cell plasma membrane. The H_{II} phase consists of cylindrical tubes arranged in a two-dimensional hexagonal lattice, where each tube is composed of a central water channel wrapped by a lipid monolayer with negative mean curvature ($c_1 = 0$, $c_2 < 0$) and zero Gaussian curvature. Finally, the L_α phase consists of locally flat stacks of bilayers which have zero curvature everywhere ($c_1 = c_2 = 0$). From the results above, it is clear that the M2 protein can induce NGC, the type of curvature that is topologically necessary for a number of membrane destabilization events including membrane budding and scission. Furthermore, the ability to generate this type of curvature persists over a range of solution conditions (Figure S9). Interestingly, addition of the anti-influenza drug amantadine, which acts by blocking M2 proton channel conductance, did not significantly alter M2 curvature generation (Figure S10). This suggests that the binding site of amantadine does not interfere with the primary curvature generating domains of the M2 protein, and therefore alternative therapeutic agents that work by antagonizing the saddle-splay curvature generating function of M2 might be used in conjunction with proton channel blockers.

To see how the amount of NGC in the Ia3d cubic generated by M2 might be realized on the neck of a bud, we extracted the average NGC, <K>, on the Ia3d minimal surface and then determined the size of a neck with corresponding K-values. For a bicontinuous cubic phase <K> is determined by the lattice parameter, a, since <K> = $-2\pi\chi/A_0a^2$, and the Euler characteristic, χ, and surface area per unit cell, A_0, are constants of the phase.[25] Using the lattice parameter for the Ia3d cubic from above we calculate <K> = −0.0403 nm^{-2}. For a constricted neck, the surface adopts the shape of a catenoid (Figure 2C),[26] another minimal surface with Gaussian curvature $K(z) = -\mathrm{sech}(z/c)^4/c^2$, where the narrowest part of the neck diameter, 2c, sets the distribution of curvature along the axis of the neck. (Catenoids are azimuthally symmetric so K is a function of z only). A catenoid with c = 5 nm has K = −0.04 nm^{-2} at the midpoint, z = 0, where the neck is most narrow and the NGC diminishes with distance from the midpoint (Figure 2D). Since spherical influenza viruses have diameters on the order of 100 nm, this implies that M2 proteins are capable of generating NGCs which would produce a neck with a diameter that is 10× smaller than the size of the virus (Figure 2B). Further analysis of the Gaussian curvature distributions on the Ia3d cubic and catenoid surfaces (see Figure S11 and discussion therein) reveals that this estimate is likely conservative for two reasons: First, the distribution of Gaussian curvature on the Ia3d peaks at a value that is significantly more negative than the average Gaussian curvature on the Ia3d surface, <K>. Since M2 proteins induce these cubic phases via NGC generation, we expect them to preferentially occupy the sites with higher NGC. Second, the distribution of NGC on a cubic phase is much more uniform compared with the distribution of NGC on the catenoid. The catenoid has appreciable NGC only in the

dx.doi.org/10.1021/ja400146z | J. Am. Chem. Soc. 2013, 135, 13710−13719

vicinity of the narrowest point on the neck (the curvature decreases exponentially away from the high NGC catenoid midpoint). This means NGC generating proteins like M2 only need to generate substantial NGC in the neck region of a membrane bud, while in order to maintain a cubic phase, the M2 proteins must arrange themselves throughout the lattice. In the biologically relevant discrete budding event, M2 proteins are free to concentrate in the NGC-rich region of the neck. All of these observations support a link between the ability of M2 proteins to generate amounts of NGC that are sufficient to drastically constrict the neck of the bud and empirical evidence that M2 can drive budding and scission in cells.

We constructed SUVs with ternary DOPE/DOPC/DOPS lipid compositions in order to examine how varying the biophysical properties of membranes affected the ability of M2 to restructure vesicles (Figure 3A,C). The intrinsic curvature of the monolayer was modified, since this parameter depends on the molecular shapes of the constituent lipid molecules. The monolayer intrinsic curvature can be approximated as the molecular area-weighted sum of the intrinsic curvature values of the constituent lipids.[27] For example, lipids with small headgroups and bulky tails are called negative intrinsic curvature lipids ($c_0 < 0$) and enriching a membrane with these lipids will move the monolayer intrinsic curvature toward negative values. In particular, we examined the relationship between membrane intrinsic monolayer curvature and M2 phase behavior by fixing the amount of anionic DOPS (c_0 = 0.07 nm^{-1})[28] at 20% and varying the relative amounts of zwitterionic DOPE (intrinsic curvature, $c_0 = -0.35 - -0.44$ nm^{-1})[29−31] and DOPC ($c_0 = -0.06$ nm^{-1}).[32] The general trend with decreasing DOPE/DOPC was the suppression of nonlamellar inverted hexagonal and cubic phase formation. Reduction of membrane DOPE to 70% extinguished the H_{II} phase, and the correlation peaks corresponding to the cubic Ia3d diminished in intensity. At DOPE/DOPC/DOPS = 60/20/20, only the $\sqrt{6}$:$\sqrt{8}$ reflections of the Ia3d were present in coexistence with an L_α phase. Diagrams of the observed phases as a function of both peptide/lipid (P/L) ratio and membrane DOPE content (Figure 3C) showed an $L_\alpha \rightarrow Q_{II} \rightarrow H_{II}$ phase progression in membranes with increasing amounts of negative intrinsic curvature lipids,[33−36] similar to previous reports on the phase behavior of curvature-inducing membrane-active antimicrobials.[37,38] M2 proteins also generated Ia3d cubic phases in membranes enriched with the lipid dioleoylglycerol (DOG) (c_0 = −0.99 nm^{-1}),[32] instead of DOPE (Figure S12). Much less (≥25%) DOG was necessary for cubic phase generation, which is expected since the measured c_0 of DOG is substantially larger in magnitude than the measured c_0 of DOPE. Since the trends in DOG-rich membranes are exactly the same as in DOPE-rich membranes, the observed phase behaviors are not lipid species specific but are characteristic of how M2 proteins generate curvature in membranes with $c_0 < 0$ lipids. Therefore, enriching membranes with negative intrinsic curvature lipids promoted the generation of topologically active NGC and negative mean curvature by M2.

Reducing the Hydrophobicity in the M2 C-cyto Helix Attenuates NGC Generation. Previous structure−activity studies of M2 proteins have demonstrated that reducing the hydrophobicity of its C-cyto amphipathic helix inhibited membrane scission and virion release.[5] This change is expected to reduce the hydrophobic volume of the helix, but it was not clear how this change relates to the detailed geometric requirements of budding. To engage this question and to determine whether curvature deformations track with protein activity, we conducted similar SAXS assays on a penta-Ala M2 protein variant (Ala-M2), where five bulky hydrophobic amino acids (3 phenylalanine, 1 tyrosine, and 1 isoleucine, see Figure S1) on the nonpolar face of the amphipathic helix were replaced with alanines (Figure 4). Like the native M2 protein,

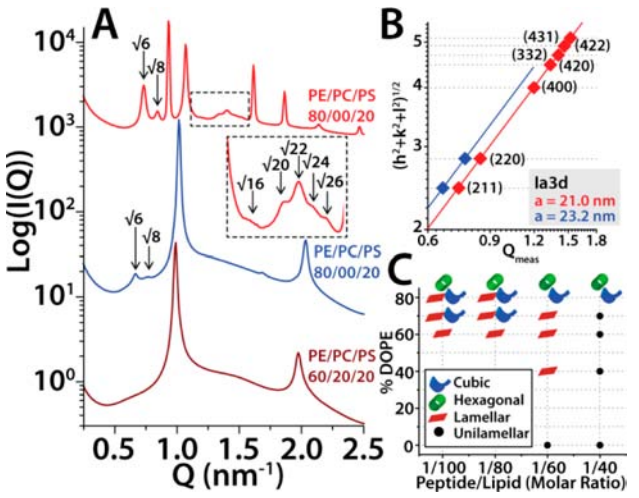

Figure 4. The Ala-M2 protein displayed reduced ability to generate NGC compared with M2. (A) Analogous SAXS spectra for Ala-M2 with DOPE/DOPC/DOPS = X/(80 − X)/20 membranes at P/L = 1/100. A DOPE concentration of X = 70% is required for Ala-M2 to induce the Ia3d cubic phase. (B) Indexation of the Ia3d cubic phases for DOPE/DOPC/DOPS = 80/20/00 (red) and 70/10/20 (blue) membrane samples. The procedure for extracting cubic phase lattice parameters is identical to Figure 3. The cubic phase lattice parameter increased with decreasing membrane DOPE concentration. (C) Phase diagram for Ala-M2. Compared to M2, Ala-AM2 showed increased propensity to induce inverted hexagonal phases, and was less able to induce cubic phases.

Ala-M2 also generated coexisting Ia3d cubic (a_{Ia3d} = 21.0 nm), H_{II} (a_{Hex} = 7.80 nm), and L_α (d = 5.87 nm) phases in membranes with 80% DOPE (Figure 4A,B). In DOPE/DOPC/DOPS = 60/20/20 membranes, unlike the native M2 protein, pure lamellar phases were observed for Ala-M2, with the NGC-rich phases completely suppressed. Comparison of the phase diagrams for M2 (Figure 3C) and Ala-M2 (Figure 4C) confirmed that decreasing the hydrophobicity in the C-cyto domain altered the membrane curvature deformations induced by M2. The native protein generated cubic phases over a significantly wider region of the phase diagram and required less membrane DOPE content to generate NGC than the penta-Ala variant. At peptide/lipid (P/L) ratios of 1/100 and 1/80, M2 induced cubic phases in DOPE/DOPC/DOPS = 60/20/20 membranes, whereas Ala-M2 induced pure lamellar phases. When the DOPE concentration was raised to 70%, although both M2 and Ala-AM2 were able to generate NGC, the native protein did so over a wider region of P/L ratios. The enhancement of NGC generation by hydrophobicity is consistent with previous reports on the effects of incorporating hydrophobic moieties into cationic polymers.[39] An additional effect of penta-Ala substitution in M2 is the increased appearance of inverted hexagonal phases with negative mean curvature. For Ala-M2 the H_{II} was present over the entire range of tested P/L ratios in DOPE/DOPS = 80/20 membranes, while the native protein generated this phase at low P/L = 1/

dx.doi.org/10.1021/ja400146z | J. Am. Chem. Soc. 2013, 135, 13710−13719

100 and 1/80. The differences in phase behavior can be explained by examining the effects that protein cationicity and hydrophobicity have on membrane curvature generation. Cationic moieties promote wrapping of anionic membranes via maximization of counterion release and therefore generate negative curvature,[24,40−42] while hydrophobicity can generate positive curvature via excluded volume effects from partial membrane insertion.[43−45] The variant Ala-M2 favors H_{II} phases since less hydrophobicity reduces positive curvature generation, whereas the hydrophobic C-cyto helix in the native M2 favors cubic phases since the orthogonal positive and negative curvatures in NGC can better accommodate greater hydrophobicity. Therefore, mutations in the M2 protein which obviate viral budding and scission reduce the ability of the protein to generate NGC, the type of curvature necessary for these processes.

M2 C-cyto Domain Is Sufficient to Generate NGC. While the full length protein can induce membrane curvature, the C-cyto domain of M2 is believed to be essential for membrane budding and scission; the C-cyto domain alone induced membrane curvature and budding in giant unilamellar vesicles.[5] Therefore, we hypothesized that it should also generate NGC in membranes. SAXS spectra confirm that the M2 C-cyto domain is sufficient for generating NGC. In DOPE/DOPS = 80/20 membranes the M2 C-cyto domain generated the Pn3m cubic phase over the entire range of tested peptide/lipid ratios (Figure 5A,C), and the domain also generated Pn3m cubics in DOG enriched membranes (Figure S13). The trends between the M2 C-cyto and the Ala-M2 C-cyto domains are similar to those observed between the full length M2 and its Ala-substituted variant. Greater amounts of Ala-M2 C-cyto domain were required before cubic phases appeared in 80% PE membranes (Figure 5B,D), demonstrating that reducing peptide hydrophobicity reduces NGC generating ability. Further comparison of both peptides at P/L = 1/100 reveals the effect of removing the 5 bulky hydrophobes from the M2 C-cyto helix (Figure 5A,B). In addition to the absence of cubic phases, the Ala-substituted variant also displayed a greater tendency to generate inverted hexagonal phases, indicated by the greater intensities of the H_{II} phase peaks compared with the lamellar phase peaks, in line with expectations that reducing the hydrophobicity in amphipathic α-helices reduces their ability to generate positive curvature. Increasing the P/L ratio supplies the system with additional hydrophobicity so that the Ala-M2 C-cyto peptides can collectively induce sufficient positive and negative curvatures to promote NGC-rich cubic phases. Moreover, at a given P/L ratio the M2 C-cyto peptide generated Pn3m cubic phases with smaller lattices parameters than the Ala-M2 C-cyto peptide, indicating that the Ala-substituted peptide also generated less NGC ($<K> \alpha 1/a^2$).[25] The data show that both M2 C-cyto and Ala-M2 C-cyto peptides can in principle generate NGC, with the former having significantly greater activity. Influenza virus budding and scission is a dynamic process that requires the concerted actions of membrane components of lipids and proteins, like M2. Throughout its progression budding likely involves spatially coordinated local changes in protein distribution and lipid composition that produce organized curvature deformations and consequently promote viral egress. The results presented here suggest that successful budding and scission depends on the degree of curvature generated, not just the kind of curvature generated; in this case whether the added NGC contribution from M2 is sufficient to drive the budding event to completion. A general effect of alanine substitutions in the M2 C-cyto domain is to reduce NGC generation, in good agreement with previous results[5] which showed that reducing peptide hydrophobicity inhibits the ability of the M2 C-cyto domain to induce membrane budding and scission. In fact, successful scission may require a minimum threshold of induced membrane NGC and accentuate the differences between M2 C-cyto and Ala-M2 C-cyto, thereby transforming a difference in degree into a difference in nature.

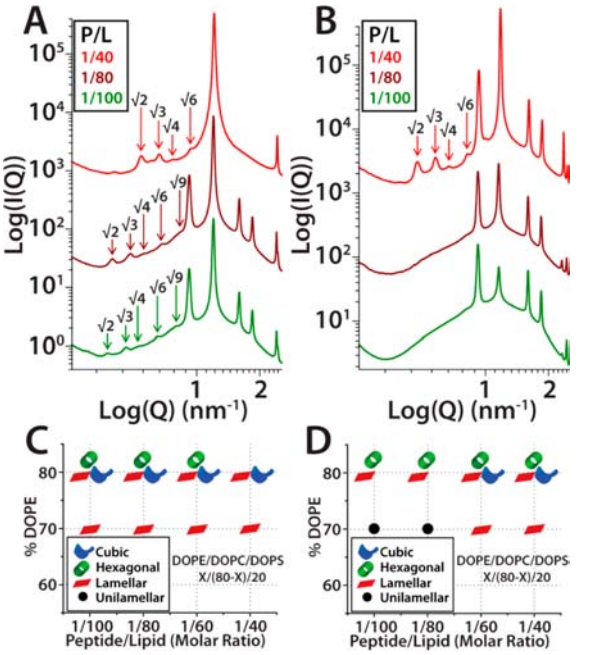

Figure 5. A peptide consisting of the M2 cytoplasmic amphipathic α-helix (45−62) is sufficient to generate membrane NGC. (A) In DOPS/DOPE = 20/80 membranes the M2 C-cyto peptide induced Pn3m cubic phases over a variety of P/L ratios. The shift of the cubic phase reflections to higher Q-values with increasing P/L shows that increased amounts of peptide generate Pn3m cubics with smaller lattice parameters. (B) Compared to the native peptide, the penta-Ala substituted M2 C-cyto showed reduced ability to generate NGC. At P/L = 1/100 and 1/80, Ala-M2 C-cyto induced only lamellar and inverted hexagonal phases; the Pn3m cubic appeared at higher P/L ratios only. (C,D) The phase diagrams for M2 C-cyto and Ala-M2 C-cyto. The native M2 C-cyto peptide showed better membrane restructuring ability than the penta-Ala variant and generated NGC over a wider region of the phase diagram.

Comparison of M2 C-cyto Peptides and Antimicrobial Peptides. The 18 amino acid peptide representing the M2 C-cyto domain contains a high proportion of cationic residues (2K, 3R, and 1H) and hydrophobic residues (4F, 2L, 1I, and 1Y) and is facially amphipathic under α-helical conformation. This is similar to the fundamental structural motif of membrane active antimicrobials (AMPs) cationic, amphipathic peptides (range from +4 to +9 net charge with >30% hydrophobic amino acids) which share a common ability to disrupt and destabilize cell membranes.[46,47] The induction of nonlamellar cubic and inverted hexagonal phases by M2 C-cyto domain peptides is also reminiscent of the general tendency of AMPs to generate topologically active curvatures in membranes.[48] For AMPs the geometric requirement that they generate, both the negative and positive curvature in NGC, further constrains their structural motif in the form of a collective pattern in the distribution of cationic residues (Lys/Arg) relative to their

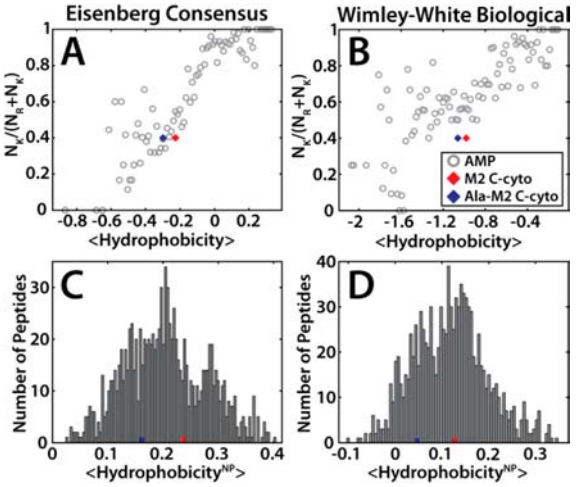

Figure 6. The amino acid composition of the M2 C-cyto peptide is similar to membrane active antimicrobial peptides. Since arginine can generate both positive and negative curvature, while lysine generates negative curvature only and hydrophobicity generates positive curvature only, the requirement that AMPs generate NGC implies that a decrease in peptide arginine content (N_R) can be offset by an increase in lysine (N_K) plus hydrophobicity. (A,B) The positive relationship between lysine and average hydrophobicity for 1080 AMPs (gray circles) using the Eisenberg consensus[49] and Wimley–White biological[50] hydrophobicity scales, respectively. The M2 C-cyto peptide (red) tends to be more hydrophobic than an average AMP with equivalent Lys/Arg ratio, and the Ala-M2 C-cyto (blue) is less hydrophobic than WT. (C,D) Histograms comparing the distribution of average AMP hydrophobicities (gray bars) with those of C-cyto domain peptides (M2 C-cyto red square, Ala-M2 C-cyto blue square) accounting for only the hydrophobic residues. (C) uses Eisenberg consensus scale, and (D) uses the Wimley–White biological scale. Both M2-derived peptides lie within the hydrophobic range of AMPs and alanine substitution results in a less hydrophobic C-cyto domain.

hydrophobic content (Figure 6).[48] Since the M2 C-cyto domain generates similar membrane curvatures as AMPs, we expect its cationicity and hydrophobicity to be in line with the observed trends for AMP sequences.

Quantitative comparisons of the amounts of cationic and hydrophobic residues (Figure 6) used by the M2 C-cyto peptide and the Ala-M2 C-cyto peptide show that their compositions are similar to AMPs. The distances of both C-cyto peptide constructs from the AMP trendlines (Figure 6A,B) are much smaller than the variations in the average hydrophobicity (<hydrophobicity>) and lysine versus arginine content ($N_K/(N_R + N_K)$) for all AMPs. Overall, the position of the M2 C-cyto domain relative to the AMP trendline shows that it is more hydrophobic or arginine-rich than an average AMP with set amount of Lys/Arg or hydrophobicity, respectively (Figure 6A,B). Replacing three phenylalanines, the isoleucine, and the tyrosine in the C-cyto domain with alanines decreases the average peptide hydrophobicity, resulting in a left shift of the Ala-M2 C-cyto peptide relative to the native one. The change in average hydrophobicity is not large. This is consistent with observations that the Ala-substituted variant can still generate NGC curvature, albeit over a significantly more limited range of conditions compared to the M2 C-cyto peptide. However, these calculations take into account all of the amino acids in a peptide and consequently can be swayed by the contributions from the polar and charged amino acids. When we isolate the specific contribution from nonpolar amino acids by considering only the hydrophobic residues in peptides (see Materials and Methods in SI), the C-cyto domain lies within the range of hydrophobicities for AMPs, and alanine substitution results in a sizable reduction in C-cyto domain peptide hydrophobicity (Figure 6C,D). Our results suggest that peptides which share cationic and hydrophobic features will likewise induce similar curvature deformations in membranes.

The M2 protein displays similar membrane curvature generating properties despite the fact that its role in influenza virus budding and scission is dissimilar to the biological function of AMPs which are involved in host defense as direct microbicides via multiple mechanisms of membrane disruption including pore formation[43,46,47,51−55] as well as blebbing, budding, and vesicularization.[56,57] While all of these processes require saddle-splay curvature, clearly, the 'monolayer' saddle-splay curvature found in a lipidic pore is different than the 'bilayer' saddle-splay curvature found at the base of a bud. Rather than focus on the differences between these two structures, we concentrate on what they have in common. From the perspective of curvature, the difference between the two situations is a difference of degree rather than a difference of kind. Transmembrane pores have NGC in the pore formed by joining the opposing membrane leaflets into a single monolayer surface. Before scission the neck of a budding event (Figure 2B,C) is equivalent to a so-called fusion pore[36] characterized by distinct inner and outer membrane leaflets with NGC on both surfaces of the bilayer. In the vicinity of the pore, the region of high NGC, a monolayer pore can be viewed as an extreme form of the bilayer pore. Consistent with this, we observe that many membrane-active molecules which share a common ability to destabilize cell membranes can generate NGC, and the phase behaviors of these membrane-active molecules and the M2 C-cyto peptide are similar.[38,39,48,58,59] Interestingly, the pore-forming peptide melittin can induce budding in phase separated GUVs consisting of multicomponent membranes.[60] Lipid composition also strongly affects both the propensity of M2 proteins to induce NGC as well as how this curvature is morphologically expressed in membranes. In liquid disordered (L_d) liquid ordered (L_o) phase separated GUVs, modeled after the lift raft domains in plasma membranes which mediate influenza egress,[61] M2 proteins partitioned into the L_d phase and clustered at the phase boundary[5] by modifying the line tension between coexisting phases. NGC generating proteins, such as M2, are expected to segregate naturally to regions on the membrane where curvature friendly volume discontinuities exist like at phase boundaries. This localization also organizes M2 proteins at the specific site where NGC is required for budding out L_o domains. Therefore, while the generation of saddle-splay membrane curvature can be manifested in different structural outcomes, it is an important underlying mechanism of activity.

Recent work has proposed potential roles played by amphipathic helices with compositions similar to the C-cyto domain in driving membrane scission. In the related field of membrane-remodeling proteins used by eukaryotic cells to generate small vesicle transport carriers, the ability of proteins to stabilize membrane necks instead of constricting them to induce scission has been related to the contrasting curvature-inducing propensities of the protein scaffold and its terminal amphipathic helices that partially insert into membranes.[21] The study showed that epsin proteins which predominantly interact with membranes via insertion of amphipathic helices tend to destabilize necks and cause scission, while the concave scaffold

of BAR domains can act as an antagonist and, instead, stabilize the saddle-splay curvature on membrane necks. This is consistent with our model.

M2TM-cyto Peptides Generate NGC Over a Wide Range of Lipid Compositions. The full length M2 protein and its C-cyto domain display differences in curvature generating ability. For example, while the native M2 generated cubic phases in membranes with DOPE concentrations as low as 60% (Figure 3C), the C-cyto domain alone required higher (>70%) DOPE content (Figure 5B) in order to generate NGC. This suggests that other domains in M2 influence curvature generation. We assayed the contributions from the membrane associated portion of M2 by probing the curvature deformations induced by a peptide consisting of the transmembrane helix plus the C-cyto domain (M2TM-cyto) (Figure 7). Cubic phases were observed over the entire range of lipid

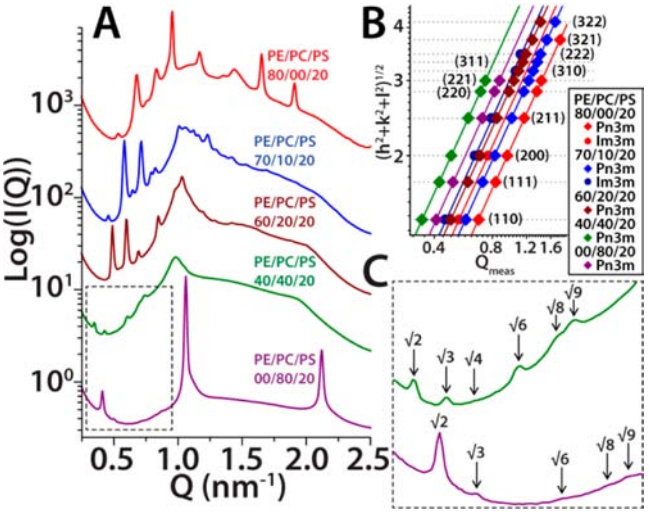

Figure 7. The M2TM-cyto peptide generated NGC over the entire range of tested lipid compositions. (A) In DOPE/DOPC/DOPS = X/(80 − X)/20 membranes, M2TM-cyto induced the coexisting Im3m and Pn3m cubic phases in PE-rich, $X \geq 70\%$ membranes, while at lower concentrations of $c_0 < 0$ lipids the Pn3m phase was observed. In general, at fixed P/L, the reflections from the Pn3m shift to lower Q-values with decreasing membrane PE concentration. P/L = 1/60 for all membrane compositions except PE/PC/PS = 00/80/20 which is at P/L = 1/40. (B) Indexation of the Pn3m and Im3m cubic phases in (A). A left shift of trendlines indicates cubic phases with larger lattice parameters. (C) Close-up view of the Pn3m cubic phase peaks in low-PE membrane spectra from (A).

compositions tested. Furthermore, changes in the lattice parameters with lipid concentration are consistent with the ability of M2TM-cyto to generate NGC. For example, at P/L = 1/60, in PE-rich DOPE/DOPS = 80/20 membranes, M2TM-cyto generated two sets of peaks with characteristic ratios, $\sqrt{2}:\sqrt{3}:\sqrt{4}:\sqrt{6}:\sqrt{8}:\sqrt{9}$ and $\sqrt{2}:\sqrt{4}:\sqrt{6}:\sqrt{8}:\sqrt{10}:\sqrt{12}$ which index to Pn3m and Im3m cubic phases[23,35] with lattice parameters, a_{Pn3m} = 13.1 nm and a_{Im3m} = 16.5 nm, respectively, as well as a third set which corresponds to an H_{II} with lattice parameter a_{Hex} = 7.6 nm (Figure 7B). The ratio of lattice parameters for the Pn3m and Im3m is a_{Im3m}/a_{Pn3m} = 1.276, close to the Bonnet ratio of 1.279 for coexisting cubics,[23] a trend we find for all coexisting cubic phases in this study. In membranes with 70% DOPE, Pn3m and Im3m phases were observed with lattice parameters, a_{Pn3m} = 15.3 nm and a_{Im3m} = 19.5 nm. These lattice parameters are larger than those for the 80% DOPE membranes, indicating that reduction of membrane PE causes a corresponding reduction of NGC (see Figure S14 for surface plots of average NGC as a function of P/L and % DOPE, i.e., <K> (P/L, %DOPE)). Indeed, the overall tendency is toward smaller amounts of induced NGC with decreased membrane DOPE content, as easily visualized by the shift in the correlation peak positions toward lower Q values (and therefore larger lattices). The direct correspondence between high amounts of NGC and increased concentrations of negative intrinsic curvature lipids is in agreement with theoretical[34,36] and experimental[33,48,62,63] studies which showed that cubic phases are more difficult to generate in membranes with reduced amounts of $c_0 < 0$ lipids. However, unlike M2 and its C-cyto domain, the presence of elevated amounts of negative intrinsic curvature lipids is not required for the M2TM-cyto peptide to generate saddle-splay membrane curvature.

Analogous experiments on Ala-M2TM-cyto showed similar trends to those observed between the other native M2 versions and their penta-Ala variants (Figure 8). At P/L = 1/60, in 80%

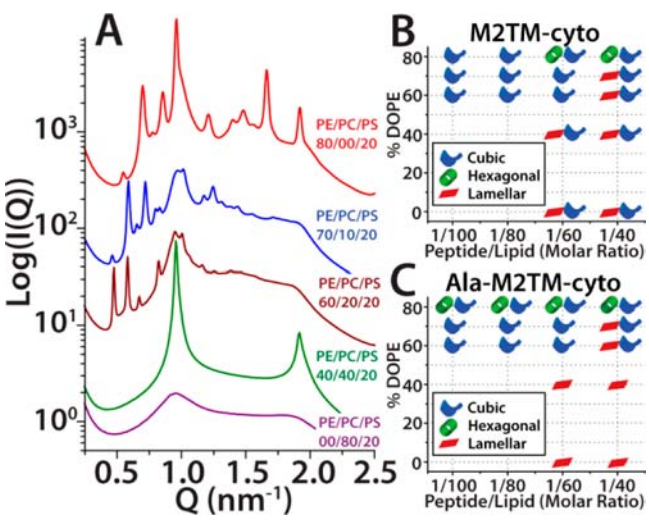

Figure 8. The Ala-M2TM-cyto peptide variant generated NGC over a smaller range of lipid compositions compared with M2TM-cyto. (A) At P/L = 1/60, Ala-M2TM-cyto induced coexisting Im3m and Pn3m cubic phases in DOPE/DOPC/DOPS = 80/00/20 and 70/10/20 membranes and 60/20/20 membranes induced a pure Pn3m cubic. In membranes with reduced DOPE, only lamellar phases were observed. The phase diagrams for (B) M2TM-cyto and (C) Ala-M2TM-cyto peptides with ternary DOPE/DOPC/DOPS = X/(80 − X)/20 lipid compositions. The native M2TM-cyto peptide generated NGC over a wider region of the phase diagram, while the Ala-substituted version displayed greater ability to generate inverted hexagonal phases.

DOPE membranes, Ala-M2TM-cyto generated Pn3m and Im3m cubic phases with lattice parameters, a_{Pn3m} = 12.7 nm and a_{Im3m} = 16.2 nm, along with an H_{II} with lattice parameter a = 7.6 nm (see Figure S15 for indexation). When the membrane DOPE content was lowered to 70%, the coexisting Pn3m and Im3m cubic phase lattice parameters increased to a_{Pn3m} = 15.1 nm and a_{Im3m} = 19.2 nm, just like for M2TM-cyto. However, unlike M2TM-cyto which produced cubic phases over all tested lipid compositions, the penta-Ala mutant required a higher threshold concentration (>40% DOPE) of negative intrinsic curvature lipids to induce NGC and produced only lamellar phases with lattice parameters d = 6.2 and 6.4 nm in DOPE/DOPC/DOPS = 40/40/20 and 00/80/20 membranes, respectively (Figure 8B,C). The reduced ability to induce

dx.doi.org/10.1021/ja400146z | J. Am. Chem. Soc. 2013, 135, 13710−13719

cubic phases by all the penta-Ala variants demonstrates that the attenuation of NGC from decreasing the hydrophobicity of the C-cyto helix is a general characteristic of the M2 protein.

The strong changes in phase behavior between the full length M2 protein, the M2TM-cyto peptide, and the C-cyto domain peptide, suggest that protein domains distinct from the primary curvature generating C-cyto domain can significantly affect membrane curvature. For instance, the native M2 generated a cubic phase (Ia3d) in membranes with elevated levels of DOPE, while the M2TM-cyto generated cubic phases (Pn3m and Im3m) over the entire range of DOPE membrane content. Therefore, removing the N-terminal extracellular domain and the C-terminal tail of the protein provokes a change in the range of lipid compositions over which cubics are observed. Interestingly, compared to the C-cyto domain, the M2TM-cyto showed much greater NGC generating ability even though the M2 transmembrane domain alone does not generate NGC (see Figure S17 for M2 TM SAXS spectra). While the large amount of hydrophobicity present in M2TM-cyto can induce correspondingly large amounts of curvature, the insertion state of the TM domain must be considered when assessing its role in membrane curvature generation. The curvature generated by a hydrophobic α-helix oriented parallel to the membrane surface depends on its membrane insertion depth,[45] and the curvature generated by a helix in a parallel state will generally be different than the curvature generated by a helix oriented normal to the surface, the presumed alignment of the TM domain. Also, tetramerization of M2TM-cyto peptides can have the additional effects such as localizing and arranging the curvature generating C-cyto domains to promote NGC in a manner that the uncoordinated C-cyto domain peptides cannot duplicate. A better understanding of how these different curvature producing mechanisms are integrated into the net membrane curvature generated by an M2 proton channel requires incorporating the structural features of M2 into the model.

How Different Membrane Curvature Generating Elements Work Together in M2. The geometric shape of the membrane-associated domains in the M2 proton channel (Figure 1) couples to the curvature generating abilities of its C-terminal amphipathic helices to generate high amounts of saddle-splay curvature. Transmembrane proteins can act as wedge-like inclusions and bend the membrane according to the volume excluded by the membrane-associated regions of the protein.[44,64] Since the M2 proton channel excludes different amounts of volume in the two monolayer leaflets, its presence in the bilayer will give rise to membrane curvature (Figure 1B,C). This wedge effect will follow the tetrameric organization of the proton channel and generate roughly symmetric membrane curvature ($c_1 \approx c_2$). A membrane neck has saddle-shaped curvature, so the wedge curvature can align with the curvature along one direction of the neck. However, the curvature generating tendencies of the four C-cyto helices break the wedge symmetry and thereby further modify the net membrane curvatures generating by the M2 proton channel (e.g., by amplifying the wedge effect when its direction is along the neck and canceling out the effect when it opposes the neck curvature). In this way the total membrane curvature induced by the M2 proton channel will promote the high amounts of asymmetric saddle-splay curvature (c_1 and c_2 have opposite signs) needed for scission. Consistent with this hypothetical picture, we observe that the transmembrane domain can amplify NGC from the amphipathic helix alone. Based on the above explanation for the different curvature generating abilities of arginine, lysine, and hydrophobicity in AMPs, we expect that cationic, amphipathic helices like the C-cyto will tend to generate positive membrane curvature parallel to the helix and generate negative membrane curvature (wrapping) around the helix. Experiments on the AMPs magainin, melittin, and protegrin suggest the peptides adopt this orientation when they insert into the membrane and form toroidal pores,[65−68] and MD simulations observed the same orientation for hydrophobic viral fusion peptides on membrane stalks.[69] Therefore, while rules for designing curvature generating peptides should provide stand-alone optimized modules,[48,58] when they are integrated into a multifunctional protein the cross-talk from other domains must be accounted for when optimizing structure−function relationships. Conversely, curvature generating modules which have been optimized to work in a protein may not work as well in isolation. Taken together, these results provide a good example of how peripheral domains can act synergistically with amphiphilic domains to induce membrane curvature.

■ CONCLUSION

In summary, we have shown that the M2 protein from the influenza A virus generated NGC in lipid membranes. As NGC is topologically necessary for virion budding and scission, the generation of high NGC by M2 provides the protein with a robust mechanism to mediate virion release. A penta-Ala M2 variant that is known to have poor ability to induce budding and scission showed significantly reduced ability to generate NGC. The C-cyto domain of M2 is sufficient to generate NGC. This is consistent with its pivotal role in viral budding and scission. While the C-cyto domain alone can generate NGC, its ability is reduced compared with the full length M2 protein and the M2TM-cyto peptide variant, suggesting that other portions of the protein influence curvature generation. These results imply that cross-talk between the different domains occurs in multifunctional proteins like M2 which has implications for engineering curvature generating proteins. Finally, as NGC generation by M2 is necessary for the budding and release in the replication cycle of the influenza virus, inhibiting this type of curvature represents a possible strategy for antiviral drug design.

■ EXPERIMENTAL SECTION

Liposome Preparation for X-ray Measurements. Liposomes were prepared as described previously.[48] Briefly, 1,2-dioleoyl-*sn*-glycero-3-phosphocholine (DOPC) (CAS no. 4235-95-4), 1,2-dioleoyl-*sn*-glycero-3-phosphoethanolamine (DOPE) (CAS no. 4004-5-1), and 1,2-dioleoyl-*sn*-glycero-3-phospho-L-serine (sodium salt) (DOPS) (CAS no. 90693-88-2) lyophilized lipids from Avanti Polar lipids were used without further purification. Small unilamellar vesicles (SUVs) were prepared by sonication. Individual stock solutions of DOPS, DOPC, and DOPE were prepared in chloroform at ∼20 mg/mL. Ternary mixtures of these lipids were prepared at mass ratios, e.g., DOPS/DOPE/DOPC = 20/40/40 corresponds to a 1:2:2 mass ratio. Chloroform was evaporated under N_2, and the mixtures were further dried by overnight desiccation under vacuum. The dried lipids were resuspended the following day in 100 mM NaCl or in Millipore H_2O. Solutions were incubated at 37 °C for 12−24 h and then sonicated until clear. SUVs were obtained via extrusion (0.2 μm pore Nucleopore filter).

SAXS Experiments. For samples made with the full length M2 protein, the C-cyto domain, the M2TM-cyto peptide, and their alanine-substituted variants, protein, and peptide stock solutions were suspended in either 100 mM NaCl or in Millipore H_2O. Lipids were

thoroughly mixed with proteins/peptides at specific protein/peptide to lipid ratios (P/L) in 100 mM NaCl. The poor solubility of the M2 transmembrane (TM) peptide necessitated different methodology. Two approaches were used to ensure consistency: (1) M2 TM dissolved in ethanol was added to eppendorf cups and then desiccated overnight to remove solvent. Stock solutions of 100 mM NaCl and lipids at specific P/L ratios were added to the dried peptide, and the resulting samples were mixed vigorously. (2) M2 TM was first dissolved in DMSO at concentration of ~20 mpg, then the solution was diluted with Millipore H_2O. Lipids and NaCl stock solutions were then thoroughly mixed with the peptide solution at specific P/L ratios. The drawback of the first method is uncertainty about resolubilization of the peptide, while DMSO from the second method can enhance pore formation, fusion, and other nonlamellar processes in lipid membranes.[70] Samples from both methods showed similar scattering spectra. For amantadine samples, amantadine from Sigma-Aldrich (CAS no. 768-94-5) was used without further purification and suspended in 100 mM NaCl. Amantadine and M2 proteins/peptides were first mixed together, followed by the addition of lipids. The salt concentration of all samples was 100 mM NaCl.

Sample solutions were hermetically sealed in quartz capillaries (Hilgenberg GmbH, Mark-tubes, code no: 4017515). SAXS experiments at synchrotron sources were conducted at the Stanford Synchrotron Radiation Laboratory (BL 4-2) and the Advanced Light Source (beamline 7.3.3). Monochromatic X-rays with energies 9−11 keV were used at SSRL and 10 keV at ALS. The scattered radiation was collected using a Rayonix MX225-HE detector (pixel size, 73.2 μm) at SSRL and a Pilatus 100k detector (pixel size, 172 μm). Samples were also measured at the California NanoSystems Institute (CNSI) at UCLA using an in house setup. A compact SAXS light source (Forvis Technologies, Inc.) was used in conjunction with a mar345 image plate detector (pixel size, 150 μm). Identical samples were prepared and measured at multiple sources to check for and ensure mutual consistency. The 2D SAXS powder patterns were integrated using the Nika 1.48 package[71] for Igor Pro 6.21 and FIT2D.[72]

SAXS Data Fits. A similar approach to the one described previously was used to determine cubic phase and hexagonal phase lattice parameters.[38] Q positions of the diffraction peaks were determined by visual inspection of the integrated $\log(I(Q))$ vs Q SAXS data using Origin Lab graphing software. The measured peak Q positions, Q_{meas}, were tabulated, and their ratios were compared against the ratios of the permitted reflections for different crystal phases to determine which phases were present in the sample. Once the crystal phase was determined its lattice parameter was calculated by a linear trendline fit of the measured, assigned peak Q positions, $Q_{(hkl)}^{meas}$, where h, k, l are the Miller indices versus their assigned reflections. For a powder averaged cubic phase $Q_{(hkl)} = 2\pi\sqrt{(h^2 + k^2 + l^2)}/a$ and for a hexagonal phase $Q_{(hk)} = (4\pi/\sqrt{3})\sqrt{(h^2 + k^2 + hk)}/a$. Therefore, we performed linear fits of $Q_{(hkl)}^{meas}$ versus $\sqrt{(h^2 + k^2 + l^2)}$ for Q_{II} phases or $Q_{(hkl)}^{meas}$ versus $\sqrt{(h^2 + k^2 + hk)}$ for H_{II} phases. The slope of the linear fit, M, was used to determine cubic ($M = 2\pi/a$) and hexagonal ($M = 4\pi/\sqrt{3}a$) lattice parameters, respectively.

Characterization of AMP and M2 C-cyto Domain Peptides. Procedure is similar to the one described previously, and the AMP data set used here is identical to the one in our previous study that used 1080 peptides.[48] Briefly, AMPs were obtained from the online antimicrobial peptide database.[73] AMP sequences were used if they have net positive charge and have activity against Gram positive or negative bacteria. For the saddle-splay selection rule plots (Figure 6A,B), the average total hydrophobicity of peptide j is defined by

$$<\text{hydrophobicity}>_j \equiv \frac{1}{n}\sum_{i=1}^{n} w_i$$

Where n = number of amino acids in the peptide, w_i = the hydrophobicity of the i^{th} amino acid in the peptide. This value is set by the particular hydrophobicity scale used. To more easily compare across scales, the value of the apparent free energy of membrane insertion for an amino acid, ΔG^{aa}_{app}, based upon the Wimley−White biological scale[50] was reversed in sign, i.e., $\Delta G^{aa}_{app} \rightarrow -\Delta G^{aa}_{app}$. The published hydrophobicity values were used for the Eisenberg consensus scale.[49]

To partition each peptide into a bin, the hydrophobic extremes for the AMP data set were determined and used to set the range of hydrophobicity scale. The range was divided into 100 equal bins. For the M peptides in a given bin, we define

$$\frac{N_K}{N_R + N_K} \equiv \frac{\sum_{j=1}^{M}(\text{number of K})_j}{\sum_{j=1}^{M}(\text{number of R})_j + (\text{number of K})_j}$$

$N_K/(N_R + N_K)$ versus <hydrophobicity> is plotted for each of the 100 bins. The M2 C-cyto domain peptide and the Ala-substituted variant were individually plotted using the same procedure.

To specifically isolate nonpolar residue contribution to peptide hydrophobicity, histograms of average hydrophobicities of AMPs and M2 C-cyto peptides were constructed by only counting the values of hydrophobic amino acids in the peptide (Figure 6C,D). This is labeled <hydrophobicity^{NP}> to distinguish this average hydrophobic contribution from just the nonpolar (NP) residues in the peptide from <hydrophobicity>, the average hydrophobicity from all peptide residues. Based on the Eisenberg consensus and Wimley−White biological hydrophobicity scales, the amino acids alanine, cysteine, phenylalanine, leucine, isoleucine, methionine, tryptophan, tyrosine, and valine are considered NP or hydrophobic. To calculate <hydrophobicity^{NP}> for a peptide the above equation is used with the additional constraint that the i^{th} amino acid must be A, C, F, L, I, M, W, Y, or V in order for its w_i hydrophobic value to be added to the sum. The summation normalization factor, n, is still the total number of amino acids in the peptide. For the AMPs histograms 100 bins were used. The hydrophobic values for the M2 C-cyto peptides were calculated in an identical manner and superimposed on the AMP histogram.

■ ASSOCIATED CONTENT

Ⓢ Supporting Information

M2 sequences used in this study, lattice parameters of the phases induced by M2 proteins and <K> values, M2-membrane SAXS spectra in different buffers, M2-Amantadine-membrane SAXS scattering spectra, NGC distributions on Ia3d cubic and catenoid surfaces, SAXS spectra of M2 and M2-cyto with DOG/DOPC/DOPS membranes, M2TM-cyto and Ala-M2TM-cyto plots of <K>(P/L,%DOPE), indexation of Ala-M2TM-cyto cubic phases, and M2 TM-membrane SAXS spectra. This material is available free of charge via the Internet at http://pubs.acs.org.

■ AUTHOR INFORMATION

Corresponding Authors

gclwong.ucla@gmail.com
william.degrado@ucsf.edu

Author Contributions

⊥These authors contributed equally.

Notes

The authors declare no competing financial interest.

■ ACKNOWLEDGMENTS

X-ray research was carried out at the Stanford Synchrotron Radiation Lightsource, a Directorate of SLAC National Accelerator Laboratory and an Office of Science User Facility operated for the U.S. Department of Energy Office of Science by Stanford University, the Advance Light Source supported by the Director, Office of Science, Office of Basic Energy Sciences, of the U.S. DOE under contract no. DE-AC02-05CH11231 and at the UCLA CNSI. This work is supported by NIH grants 1UO1 AI082192-01 (G.C.L.W.), GM56416 (W.F.D.), and

AI74571 (W.F.D.), NSF grant DMR1106106 (G.C.L.W.), and by the MRSEC program of NSF to the LRSM of the University of Pennsylvania.

REFERENCES

(1) Chen, B. J.; Lamb, R. A. *Virology* **2008**, *372*, 221.
(2) Carlton, J. G.; Martin-Serrano, J. *Biochem. Soc. Trans.* **2009**, *37*, 195.
(3) Pornillos, O.; Garrus, J. E.; Sundquist, W. I. *Trends Cell Biol.* **2002**, *12*, 569.
(4) Bruce, E. A.; Medcalf, L.; Crump, C. M.; Noton, S. L.; Stuart, A. D.; Wise, H. M.; Elton, D.; Bowers, K.; Digard, P. *Virology* **2009**, *390*, 268.
(5) Rossman, J. S.; Jing, X.; Leser, G. P.; Lamb, R. A. *Cell* **2010**, *142*, 902.
(6) Wang, J.; Qiu, J. X.; Soto, C.; DeGrado, W. F. *Curr. Opin. Struct. Biol.* **2011**, *21*, 68.
(7) Helenius, A. *Cell* **1992**, *69*, 577.
(8) Ma, C.; Polishchuk, A. L.; Ohigashi, Y.; Stouffer, A. L.; Schoen, A.; Magavern, E.; Jing, X.; Lear, J. D.; Freire, E.; Lamb, R. A.; DeGrado, W. F.; Pinto, L. H. *Proc. Natl. Acad. Sci. U.S.A.* **2009**, *106*, 12283.
(9) Kochendoerfer, G. G.; Salom, D.; Lear, J. D.; Wilk-Orescan, R.; Kent, S. B. H.; DeGrado, W. F. *Biochemistry* **1999**, *38*, 11905.
(10) Salom, D.; Hill, B. R.; Lear, J. D.; DeGrado, W. F. *Biochemistry* **2000**, *39*, 14160.
(11) Cady, S. D.; Luo, W.; Hu, F.; Hong, M. *Biochemistry* **2009**, *48*, 7356.
(12) Rossman, J. S.; Jing, X.; Leser, G. P.; Balannik, V.; Pinto, L. H.; Lamb, R. A. *J. Virol.* **2010**, *84*, 5078.
(13) Martin, K.; Helenius, A. *Cell* **1991**, *67*, 117.
(14) Nguyen, P. A.; Soto, C. S.; Polishchuk, A.; Caputo, G. A.; Tatko, C. D.; Ma, C.; Ohigashi, Y.; Pinto, L. H.; DeGrado, W. F.; Howard, K. P. *Biochemistry* **2008**, *47*, 9934.
(15) Rossman, J. S.; Lamb, R. A. *Virology* **2011**, *411*, 229.
(16) Stouffer, A. L.; Acharya, R.; Salom, D.; Levine, A. S.; Di Costanzo, L.; Soto, C. S.; Tereshko, V.; Nanda, V.; Stayrook, S.; DeGrado, W. F. *Nature* **2008**, *451*, 596.
(17) Schnell, J. R.; Chou, J. J. *Nature* **2008**, *451*, 591.
(18) Cady, S. D.; Schmidt-Rohr, K.; Wang, J.; Soto, C. S.; DeGrado, W. F.; Hong, M. *Nature* **2010**, *463*, 689.
(19) Sharma, M.; Yi, M.; Dong, H.; Qin, H.; Peterson, E.; Busath, D. D.; Zhou, H.-X.; Cross, T. A. *Sci. Signaling* **2010**, *330*, 509.
(20) Zhou, H.-X.; Cross, T. A. *Protein Sci.* **2013**, *22*, 381.
(21) Boucrot, E.; Pick, A.; Çamdere, G.; Liska, N.; Evergren, E.; McMahon, H. T.; Kozlov, M. M. *Cell* **2012**, *149*, 124.
(22) Squires, A. M.; Templer, R. H.; Seddon, J. M.; Woenckhaus, J.; Winter, R.; Finet, S.; Theyencheri, N. *Langmuir* **2002**, *18*, 7384.
(23) Shearman, G. C.; Ces, O.; Templer, R. H.; Seddon, J. M. *J. Phys.: Condens. Matter* **2006**, *18*, S1105.
(24) Schmidt, N.; Mishra, A.; Lai, G. H.; Wong, G. C. L. *FEBS Lett.* **2010**, *584*, 1806.
(25) Harper, P. E.; Gruner, S. M. *Eur. Phys. J. E: Soft Matter Biol. Phys.* **2000**, *2*, 217.
(26) Kozlovsky, Y.; Kozlov, M. M. *Biophys. J.* **2003**, *85*, 85.
(27) Siegel, D. P. *Biophys. J.* **2008**, *95*, 5200.
(28) Fuller, N.; Benatti, C. R.; Peter Rand, R. *Biophys. J.* **2003**, *85*, 1667.
(29) Kooijman, E. E.; Chupin, V.; Fuller, N. L.; Kozlov, M. M.; de Kruijff, B.; Burger, K. N. J.; Rand, P. R. *Biochemistry* **2005**, *44*, 2097.
(30) Epand, R. M.; Fuller, N.; Rand, R. P. *Biophys. J.* **1996**, *71*, 1806.
(31) Chen, Z.; Rand, R. P. *Biophys. J.* **1997**, *73*, 267.
(32) Szule, J. A.; Fuller, N. L.; Peter Rand, R. *Biophys. J.* **2002**, *83*, 977.
(33) Shyamsunder, E.; Gruner, S. M.; Tate, M. W.; Turner, D. C.; So, P. T. C.; Tilcock, C. P. S. *Biochemistry* **1988**, *27*, 2332.
(34) Anderson, D. M.; Gruner, S. M.; Leibler, S. *Proc. Natl. Acad. Sci. U.S.A.* **1988**, *85*, 5364.
(35) So, P.; Gruner, S.; Erramilli, S. *Phys. Rev. Lett.* **1993**, *70*, 3455.
(36) Siegel, D. P.; Kozlov, M. M. *Biophys. J.* **2004**, *87*, 366.
(37) Yang, L.; Gordon, V. D.; Trinkle, D. R.; Schmidt, N. W.; Davis, M. A.; DeVries, C.; Som, A.; Cronan, J. E.; Tew, G. N.; Wong, G. C. L. *Proc. Natl. Acad. Sci. U.S.A.* **2008**, *105*, 20595.
(38) Schmidt, N. W.; Tai, K. P.; Kamdar, K.; Mishra, A.; Lai, G. H.; Zhao, K.; Ouellette, A. J.; Wong, G. C. L. *J. Biol. Chem.* **2012**, *287*, 21866.
(39) Schmidt, N. W.; Lis, M.; Zhao, K.; Lai, G. H.; Alexandrova, A.; Tew, G. N.; Wong, G. C. L. *J. Am. Chem. Soc.* **2012**, *134*, 19207.
(40) May, S.; Ben-Shaul, A. *Biophys. J.* **1997**, *73*, 2427.
(41) Koltover, I.; Salditt, T.; Rädler, J. O.; Safinya, C. R. *Science* **1998**, *281*, 78.
(42) Yang, L.; Liang, H.; Angelini, T. E.; Butler, J.; Coridan, R.; Tang, J. X.; Wong, G. C. L. *Nat. Mater.* **2004**, *3*, 615.
(43) Matsuzaki, K.; Sugishita, K.-i.; Ishibe, N.; Ueha, M.; Nakata, S.; Miyajima, K.; Epand, R. M. *Biochemistry* **1998**, *37*, 11856.
(44) McMahon, H. T.; Gallop, J. L. *Nature* **2005**, *438*, 590.
(45) Campelo, F.; McMahon, H. T.; Kozlov, M. M. *Biophys. J.* **2008**, *95*, 2325.
(46) Hancock, R. E. W.; Sahl, H.-G. *Nat. Biotechnol.* **2006**, *24*, 1551.
(47) Zasloff, M. *Nature* **2002**, *415*, 389.
(48) Schmidt, N. W.; Mishra, A.; Lai, G. H.; Davis, M.; Sanders, L. K.; Tran, D.; Garcia, A.; Tai, K. P.; McCray, P. B.; Ouellette, A. J.; Selsted, M. E.; Wong, G. C. L. *J. Am. Chem. Soc.* **2011**, *133*, 6720.
(49) Eisenberg, D.; Weiss, R. M.; Terwilliger, T. C.; Wilcox, W. *Faraday Symp. Chem. Soc.* **1982**, *17*, 109.
(50) Hessa, T.; Kim, H.; Bihlmaier, K.; Lundin, C.; Boekel, J.; Andersson, H.; Nilsson, I.; White, S. H.; von Heijne, G. *Nature* **2005**, *433*, 377.
(51) Brogden, K. A. *Nat. Rev. Microbiol.* **2005**, *3*, 238.
(52) Huang, H. W. *Biochemistry* **2000**, *39*, 8347.
(53) Selsted, M. E.; Ouellette, A. J. *Nat. Immunol.* **2005**, *6*, 551.
(54) Ganz, T. *Nat. Rev. Immunol.* **2003**, *3*, 710.
(55) Lehrer, R. I. *Nat. Rev. Microbiol.* **2004**, *2*, 727.
(56) Falagas, M. E.; Kasiakou, S. K. *Clin. Infect. Dis.* **2005**, *40*, 1333.
(57) Saiman, L.; Tabibi, S.; Starner, T. D.; San Gabriel, P.; Winokur, P. L.; Jia, H. P.; McCray, P. B.; Tack, B. F. *Antimicrob. Agents Chemother.* **2001**, *45*, 2838.
(58) Mishra, A.; Lai, G. H.; Schmidt, N. W.; Sun, V. Z.; Rodriguez, A. R.; Tong, R.; Tang, L.; Cheng, J.; Deming, T. J.; Kamei, D. T.; Wong, G. C. L. *Proc. Natl. Acad. Sci. U.S.A.* **2011**, *108*, 16883.
(59) Mishra, A.; Gordon, V.; Yang, L.; Coridan, R.; Wong, G. *Angew. Chem., Int. Ed.* **2008**, *47*, 2986.
(60) Yu, Y.; Vroman, J. A.; Bae, S. C.; Granick, S. *J. Am. Chem. Soc.* **2009**, *132*, 195.
(61) Chazal, N.; Gerlier, D. *Microbiol. Mol. Biol. Rev.* **2003**, *67*, 226.
(62) Prenner, E. J.; Lewis, R. N. A. H.; Neuman, K. C.; Gruner, S. M.; Kondejewski, L. H.; Hodges, R. S.; McElhaney, R. N. *Biochemistry* **1997**, *36*, 7906.
(63) Lohner, K.; Prenner, E. J. *Biochim. Biophys. Acta, Biomembr.* **1999**, *1462*, 141.
(64) Phillips, R.; Ursell, T.; Wiggins, P.; Sens, P. *Nature* **2009**, *459*, 379.
(65) Ludtke, S. J.; He, K.; Heller, W. T.; Harroun, T. A.; Yang, L.; Huang, H. W. *Biochemistry* **1996**, *35*, 13723.
(66) Yang, L.; Harroun, T. A.; Weiss, T. M.; Ding, L.; Huang, H. W. *Biophys. J.* **2001**, *81*, 1475.
(67) Yang, L.; Weiss, T. M.; Lehrer, R. I.; Huang, H. W. *Biophys. J.* **2000**, *79*, 2002.
(68) Tang, M.; Waring, A. J.; Hong, M. *J. Am. Chem. Soc.* **2007**, *129*, 11438.
(69) Fuhrmans, M.; Marrink, S. J. *J. Am. Chem. Soc.* **2011**, *134*, 1543.
(70) Notman, R.; Noro, M.; O'Malley, B.; Anwar, J. *J. Am. Chem. Soc.* **2006**, *128*, 13982.
(71) usaxs.xor.aps.anl.gov/staff/ilavsky/nika.html.
(72) www.esrf.eu/computing/scientific/FIT2D/.
(73) Wang, Z.; Wang, G. *Nucleic Acids Res.* **2004**, *32*, D590.